

Exploring the Potential of Machine Learning in Predicting Soil California Bearing Ratio Values

Xu Wu¹, Feng Lu^{2*}, Tao He¹

¹ Department of BIM Research, Nantong Institute of Technology, 226002 Nantong, China

² Nantong Huarong Construction Group Co., Ltd, 2260022 Nantong, Jiangsu, China

* Corresponding author, e-mail: nthrzj@163.com

Received: 29 October 2024, Accepted: 09 January 2025, Published online: 18 February 2025

Abstract

Accurately predicting the California Bearing Ratio (CBR) of soil is vital for civil engineering projects as it determines soil strength and stability, crucial for designing safe and durable infrastructure. Conventional methods for calculating CBR values are both expensive and time-consuming, prompting the need for more efficient approaches. This study explores the use of advanced machine learning (ML) techniques to improve workflow and productivity in CBR prediction. Specifically, the Improved Arithmetic Optimization Algorithm (IAOA) and the Bonobo Optimization Algorithm (SBOA) are applied to enhance the Stochastic Gradient Boosting Regression (SGBR) model for predicting CBR values. The SGBR model, known for its ability to handle complex datasets and nonlinear interactions, is optimized to improve predictive accuracy. Performance metrics such as the coefficient of determination (R^2), n10-index, and Root Mean Squared Error (RMSE) are used to assess the model's performance. After training, testing, and validation with relevant data, the optimized SGIA model (SGBR enhanced by IAOA) achieves impressive results, including an n10-index of 1.000, a root mean square error of 0.161, and an R^2 value of 0.981. These metrics demonstrate the SGIA model's capability to accurately forecast CBR values, offering a reliable, cost-effective alternative to traditional methods for soil evaluation in engineering applications.

Keywords

regression analysis, California bearing ratio, stochastic gradient boosting regression, self-adaptive bonobo optimization algorithm, improved arithmetic optimization algorithm

1 Introduction

Cities have been getting their resources and energy supply required for survival as in the case of living beings [1–3]. However, more methodical and sustainable resource management techniques are required because of the increasing urban inflows driven by population expansion and technological advancements [4]. A fundamental theme of this discussion is the creation of new, environmentally friendly materials that may be used in cities, with a particular focus on the building industry, which is one of the industries that use the most resources and contribute the most to environmental damage. Soil, which is mostly used in building projects like roads and pavements, is extremely stressed, which highlights how important it is to understand the characteristics and behaviors of soil to ensure sectoral sustainability. The CBR value of the subgrade has the possibility of making an extremely huge impact on the overall cost of construction by altering the thickness and depth of construction in road pavement. By means of evaluating

material strengths, the CBR penetration test calculates the bearing capability of materials that are intended to be used as the subgrade for a road during construction [5]. This ratio, which may be stated as follows, is crucial in figuring out how thick the pavement and sub-base layers are.

$$\text{CBR} = \frac{\text{Test Load}}{\text{Standard Load}} \times 100 \quad (1)$$

In this case, the "Test Load" is the force piercing a soil sample, while the "Standard Load" is the resistance provided by a standard crushed aggregate sample that offers a CBR of 100% to similar penetration. The larger value is taken up for design purposes. CBR values are usually tested at penetrations of 2.5 mm and 5 mm [6].

The design and construction of road infrastructure depend a lot on the precise evaluation of the geotechnical characteristics of the soil [7–10]. As of right now, the CBR and adjusted proctor parameters, including the maximum

dry unit weight ($\gamma_{d(\max)}$) and optimum moisture content (ω_{opt}), still have a significant influence on the characteristics of subgrades, embankments, and pavement constructions. The updated proctor parameters help review the mechanical performance of soil regarding density and moisture content-soil being important in the design of road infrastructure [11–13]. The values of CBR are conventionally used to determine subgrade bearing capacity under various saturation and compaction conditions [14–16]. This is particularly crucial as a community's level of economic development is significantly influenced by its transportation infrastructure [17–19].

The main issues in the determination of soil geotechnical characteristics, such as CBR and modified proctor parameters, are only substantial commitments of time and expense for laboratory testing, which delay the process of infrastructure design and construction. Therefore, several mathematical models using easily measurable information such as soil particle size distribution, Atterberg limits, specific gravity of solids, and plasticity index have been proposed in the literature to predict these attributes, mostly based on MLR [20, 21]. However, in cutting-edge research, computer models based on AI approaches are progressively replacing conventional mathematical models [22–24]. This change is explained by the ability of computer methods to simultaneously analyze complex correlations across large datasets, providing improved predicted accuracy [25, 26].

Because of its excellent predictive accuracy and resilience, the SGBR model was used in this work to estimate soil CBR values. In this situation, the ML model named SGBR is used because, in comparison to conventional statistical techniques, it is more accurate at making predictions and is capable of handling intricate, nonlinear interactions between input and target variables. In order to further improve the performance of the SGBR model, two optimization techniques were introduced: IAOA and SBOA. After incorporating this procedure, two new models were developed labeled as SGIA and SGSB, respectively. These added optimizers have certain merits, in that they accelerate convergence, raise the performance of the prediction, and obtain the optimal model parameters that reduce overfitting and enhance generalization skills. These hybrid models outperform the basic SGBR model because of the optimizers modifying model parameters adaptively with the aim of increasing accuracy and dependability in the forecasted values of soil CBR.

2 Study methodology

2.1 Data collection

These input variables are also essential to the ML models that come into play in predicting the CBR values. Each of these variables reveals different physical and chemical properties of soil, which, when combined, have an impact on the ability of the same to carry loads. The characteristics, when carefully collected and integrated, will also enable machine learning algorithms to predict correct and consistent values of the CBR. This can help, in geotechnical engineering, design and analyze soil stabilization and compaction processes. The typical input variables are described below:

- Ash type:
The ash used in a soil mixture may be in the form of fly ash, bottom ash, or other types of industrial ash. There are different kinds of ashes; all have various chemical and physical properties that enable them to influence the strength of the soil and its compactness, both factors that could alter the CBR values.
- Percentage of ash (%):
It is usually expressed in terms of the percentage of total weight, and the quantity of ash applied to the soil is specified. Since the quantity of ash injected into the soil changes the density of the soil, the moisture content, and its compaction, all these changes affect the CBR value. With changing types of soil and ash, increasing ash percentages will either increase or decrease soil stability.
- Liquid Limit (LL):
The water content at which the soil changes from a plastic to a liquid condition. The liquid limit is one of the basic concepts in the mechanics of soil that characterize the consistency and the potential of the deformation of soil under stress. The behavior of soil in cases of high moisture is very important for the correct prediction of CBR.
- Plastic Limit (PL):
The water in the soil makes it plastic, a term used to denote that it may be molded without breaking. The plastic limit shows cohesion and workability of the soil. It is coupled with the liquid limit to form the plasticity index which is a measure of the range of soil plasticity. Plasticity index is one of the significant tests used in determining soil strength.
- Optimum Moisture Content (OMC):
It is the percentage of moisture in a soil that is mixed with water to attain its maximum dry density upon

compaction. OMC will be important in soil compaction works as it gives the optimum moisture content which yields maximum density. Compaction at OMC has to be done properly to achieve high CBR values, which imply improved load-carrying capacity.

- **Maximum Dry Density (MDD):**
Maximum density of a soil achieved for an optimum level of compaction. MDD is the measurement that gives the degree of compaction and load-carrying capacity of soil. The higher MDD values correspond to more compact and stable soil structure, and thus normally higher CBR values will correspond to higher MDD values.

Table 1 provides minimum, maximum, average and standard deviation of the input and output data in order to give the complete statistical representation of dataset used in this research. The data dissemination and distribution could also be visually assessed through the histogram plot depicted in Fig. 1 for each input and output parameter. The most important observation from the histogram is the distribution frequency of soaking CBR values. It peaks at about 45 occurrences in the 4 to 4.5 range. This suggests that a sizable number of the soil samples have comparable load-bearing capacity when wet. It also shows a concentration of soaked CBR values around this period. Such in-depth statistical and visual assessments support the trustworthiness of predictive models by evaluating the consistency of model inputs and assisting in the understanding of underlying data patterns.

2.2 SGBR

Breiman [27] first proposed that function estimation procedures could perform better if they included randomness. He called this procedure the "bagging" procedure. Random sampling was also used in early AdaBoost implementations [28], but this was regarded as a work-around for deterministic weighting in cases where the

base learner's implementation did not support observation weights, rather than a necessary component. Following that, Breiman [29] suggested adaptive bagging, a hybrid bagging-boosting technique meant for least-squares fitting of additive expansions. This is accomplished by replacing the base learner in standard boosting processes with the matching bagged base learner that uses "out-of-bag" residuals at each step of boosting instead of the usual residuals.

Inspired by Breiman [29], to make randomization an essential part of the process, a minor adjustment was made to gradient boosting. To be more precise, a random subsample of the training data is selected from the entire training data set for each iteration. The base learner and the model update for the current iteration are then fitted using this randomly selected subsample rather than the entire sample.

Assume that $\{\pi(i)\}_1^n$ represents an arbitrary permutation of the numbers $\{1, \dots, n\}$ and that $\{y_i, x_i\}_1^n$ is the complete training data sample. Then, $\{y_{\pi(i)}, x_{\pi(i)}\}_1^{\tilde{n}}$ gives the random subsample of size $\tilde{n} < n$. Additionally, Algorithm 1 shows the procedure for stochastic gradient boosting.

The smaller the percentage $f = n/\tilde{n}$, the more random samples which will be used in subsequent iterations will differ, hence the more overall unpredictable the process will be. Using the value $f = 1/2$ is more or less the same as taking bootstrap samples at each iteration. Computation is also lowered by a factor of f when $\tilde{n} = f \times n$ is used. Reducing the value of f however, results in less data being available for training the base learner during each iteration. The variation linked to each base learner estimate will rise as a result.

2.2.1 Regression

This section examines how randomization affects the (Huber) $M_TreeBoost$ process. $M_TreeBoost$ was regarded as the preferred method among the regression procedures derived in Friedman [30] because it had the best overall performance. The default value of $\alpha = 0.9$ was assigned to the break-down parameter. For small datasets ($n = 500$), the shrinking parameter ν (Algorithm 1) was set at 0.005. The same was done for the bigger ones: ($n = 5000$), $\nu = 0.005$. Six terminal node best-first regression trees were considered as the base learner.

Each of the two error distributions pertains to a comparison of performance across the 100 target functions using different randomization levels. One hundred $\{y_i, x_i\}_1^n$ data sets were produced in accordance with

$$y_i = F^*(x_i) + \varepsilon_i. \quad (2)$$

Table 1 The statistical properties of the input variable CBR

| Variables | Category | Indicators | | | |
|------------|----------|------------|------|----------|----------|
| | | Min | Max | Avg | St. Dev. |
| Ash type | Input | 3 | 1 | 2 | 0.816497 |
| % of ash | Input | 60 | 0 | 14 | 16.49242 |
| LL | Input | 64 | 17 | 39.28452 | 10.5037 |
| PL | Input | 30.1 | 12.8 | 20.59186 | 4.547399 |
| OMC | Input | 32.5 | 8.91 | 17.70795 | 5.101843 |
| MDD | Input | 1.88 | 1.37 | 1.614429 | 0.102775 |
| Soaked CBR | Output | 6.46 | 1.86 | 3.780714 | 0.984408 |

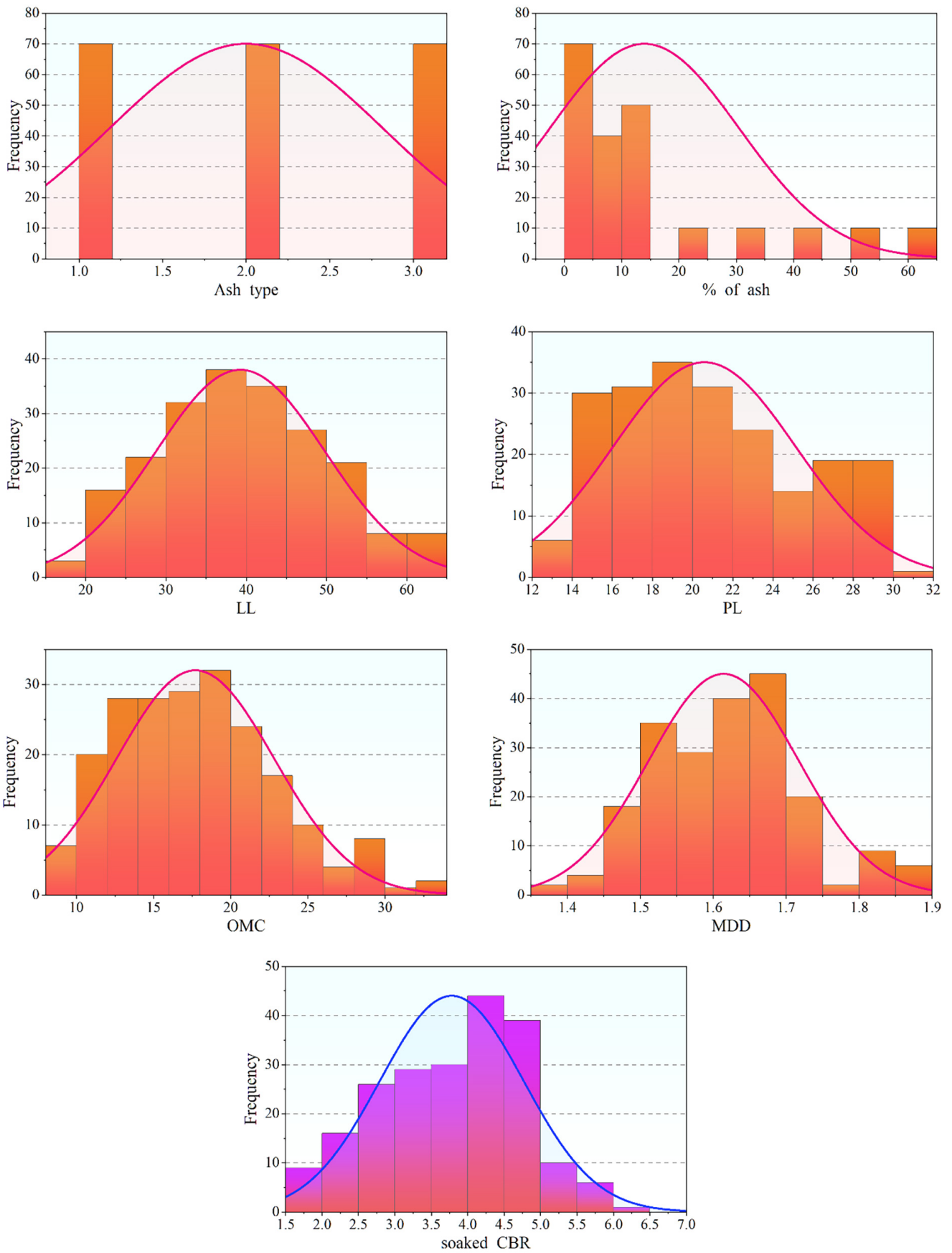


Fig. 1 A histogram plot illustrating both input and output variables

Algorithm 1 Stochastic gradient tree boost

$$F_0(x) = \arg \min_{\gamma} \sum_{i=1}^n \psi(y_i, \gamma)$$

For $m = 1$ to M do:

$$\{\pi(i)\}_1^n = \text{rand}_{\text{perm}} \{i\}_1^n$$

$$\tilde{y}_{\pi(i)m} = - \left[\frac{\partial \psi(y_{\pi(i)}, F(x_{\pi(i)}))}{\partial F(x_{\pi(i)})} \right]_{F(x)=F_{m-1}(x)}, \quad i=1, \tilde{n}$$

$$\{R_m\}_1^L = L - \text{terminal node tree}(\{\tilde{y}_{\pi(i)m}, x_{\pi(i)}\}_1^{\tilde{n}})$$

$$\gamma_{lm} = \arg \min_{\gamma} \sum_{x_{\pi(i)} \in R_m} \psi(y_{\pi(i)}, F_{m-1}(x_{\pi(i)}) + \gamma)$$

$$F_m(x) = F_{m-1}(x) + v \times \gamma_{lm} 1(x \in R_m)$$

End For

Where every one of the 100 target functions created at random is represented by $F^*(x)$. In the initial investigation, the variance was adjusted and zero mean in a Gaussian distribution was used to generate the errors ε_i .

$$E|\varepsilon| = E_x |F^*(x) - \text{median}_x F^*(x)| \quad (3)$$

Providing a signal-to-noise ratio of 1/1. In the second study, $u \sim n(0, 1)$ and $v \sim U[0, 1]$, and the errors were derived from a "slash" distribution, $\varepsilon_i = s \times (u/v)$. From Eq. (3), the signal-to-noise ratio is 1/1 after allowing for the scale factor s . The slash distribution is sometimes used as an outlier with its very heavy tails to test robustness.

2.3 Optimizers

2.3.1 SBOA

The SBOA is an evolutionary optimization technique. The behavior and mating habits of bonobos in social settings serve as its model. SBOA is distinguished by its capacity to adaptively modify its search parameters in response to population performance, allowing it to effectively achieve a balance between execution and exploration. 4 basic mating strategies are used by bonobos to create offspring: promiscuity, consortship, limited, and extra-group mating. SBOA is particularly effective in solving problems requiring the exploration of complicated nonlinear search spaces, difficult or impossible for other optimization techniques to consider [31]. Using a fixed population size and random population initialization, the SBOA is a population-based technique. The solution, known as a bonobo in the population, is used to calculate the fitness values of all bonobos. The alpha bonobo (α_b),

the highest rank in the social hierarchy of a bonobo community, is chosen because it is more fit than other bonobos in the group. Consequently, it is now considered the best option. Along with this process, SBOA parameters are also kept to their defaults. Furthermore, since bonobos oscillate between the positive and negative phases of their phase probability p_p , speculations can be drawn regarding the population diversity or selection pressure [31]. The two major governing parameters prescribed by SBOA are p_p and the sharing co-efficient (β). The aforementioned parameters may update and self-correct through repulsion-based learning in every iteration. This method relies solely on the data gathered during the search procedure. The values of both p_p and β can be found in the range 0–1. N is the quantity of answers to p_p or β from the present populace that is provided in each cycle. It is expected that these parameters will have a range of values. First, N created these parameters from a normal distribution, each having a mean (μ) and standard deviation (σ) equal to 0.5. The maximum and lowest values of the parameters can be altered. They are set to their maximum value initially. Then, they are changed, according to the requirements of the search procedure, in their range [32].

The updating of the phase probability, p_p , with the repulsion approach, follows the process given in Eq. (4).

$$P_p \text{ modified}_{\text{better}} = P_p \text{ better} + \frac{\sigma \times P_p \text{ better} \times P_p \text{ worse}}{e^{(P_p \text{ better} - P_p \text{ worse})^2}} \quad (4)$$

Generating new bonobos through different methods of mating

The mating behavior of bonobos is determined by the phase probability (p_p) parameter. The p_p has an initial value of 0.5 and is changed after each iteration.

Restrictive and promiscuous mating techniques

As Eq. (5) shows, the next generation of bonobos is generated by both promiscuous and limited mating strategies.

$$\text{new}_{b_i} = b_i + \beta_i \times \left[\begin{aligned} &(b_p - b_i) + (b_{k1} - \text{oldpop}_{k2}) \\ &+ (\text{oldpop}_{k3} - \text{badpop}_{k4}) \end{aligned} \right] \quad (5)$$

Where the i^{th} new solution is depicted by the new_{b_i} . Furthermore, the i^{th} , p^{th} , and $k1^{\text{th}}$ solutions for the current population are b_i , b_p , and b_{k1} , respectively. In the same way, the solutions for oldpop_{k2} and oldpop_{k3} are $k2^{\text{th}}$ and $k3^{\text{th}}$, respectively. The third population to be memorized is called badpop_{k4} , and it contains the 4^{th} solution of the badpop population. The i^{th} -sharing coefficient has value β_i . It is

important to note that the 4 values, $k1$, $k2$, $k3$, and $k4$, were chosen at random from the space $(1, N)$ [31]. Restrictive and promiscuous mating techniques are described below:

1. Extra-group mating technique

The solution is updated by extra-group mating if the random number is smaller than or equal to the probability of extra-group mating ($pxgm$), determined by Eqs. (6)–(8).

$$C_o = e^{\left(r_1 - \frac{1}{r_1}\right)} \quad (6)$$

$$\text{new}_{b_i}^j = b_i^j + C_o \times (E_{\max_j} - b_i^j), \quad (7)$$

if $r_2 \leq 0.5$

$$\text{new}_{b_i}^j = b_i^j + C_o \times (b_i^j - E_{\min_j}), \quad (8)$$

if $r_2 > 0.5$

An intermediary parameter is C_o . 2 unique random numbers, r_1 and r_1 , were produced in the interval 0 to 1. The j^{th} factors of the provided solution and the i^{th} bonobo of the current *populace* is $\text{new}_{b_i}^j$ [32].

2. Consort ship mating technique

To produce new offspring, the consort ship mating strategy is employed when the value of r_2 exceeds the value of ($pxgm$). Equations (9)–(15) illustrate this procedure.

$$C_1 = e^{\left(r_1 - \frac{2}{r_1}\right)} \quad (9)$$

$$\text{new}_{b_i}^j = \text{bad}_{pop_i}^j + C_1 \times (b_i^j - \text{bad}_{pop_i}^j), \quad (10)$$

if $r_3 \leq 0.5$

$$\text{new}_{b_i}^j = \text{bad}_{pop_i}^j + C_o \times (b_i^j - \text{bad}_{pop_i}^j), \quad (11)$$

if $r_4 \leq p_{p_i}$

$$dv = \text{minimum of } \left\{ 1, \frac{\left(\sum_{j=1}^d \sigma_j \right) \text{Current population}}{\left(\sum_{j=1}^d \sigma_j \right) \text{Initial population}} \right\} \quad (12)$$

$$C_2 = \text{maximum of } (2, dv \times \text{tsgsmax}) \quad (13)$$

$$C_3 = e^{\left(r_1 - \frac{C_2}{r_1}\right)} \quad (14)$$

$$\text{new}_{b_i}^j = \text{bad}_{pop_i}^j + C_3 \times (b_i^j - \text{bad}_{pop_i}^j), \quad (15)$$

otherwise

The maximum size of a group is denoted by tsgsmax , whereas C_1 , C_2 , C_3 , and dv are intermediate parameters [33].

3. Adapted boundary management methodology

The maximum bound value is assigned to the generated bonobo if it crosses with a probability of 0.5 over the top variable limit. If not, it is modified using Eqs. (16) and (17) with a 50% chance.

Similarly, if a new discovery of a bonobo is found to pass the lower bounds of the variables, then modifications will be carried out using those very equations.

$$\text{new}_{b_i}^j = r_5 \times b_i^j + (1 - r_5) \times E_{\max}^j \quad (16)$$

$$\text{new}_{b_i}^j = r_5 \times b_i^j + (1 - r_5) \times E_{\min}^j \quad (17)$$

The following is a summary of the steps involved in implementing the SBOA:

- setting up the SBOA's population size and parameters;
- an analysis of the fitness levels of every bonobo;
- the α_b 's identification;
- randomly selecting the p^{th} bonobo from the well-chosen answers.
- Is $(0, 1) \leq p_p$ a random number?
- If so, create a new bonobo by using either the restricted or promiscuous mating technique.
- If untrue, create a new generation by consort ship or extra group mating.
- Determine the alpha bonobo's fitness value and that of the new bonobos.
- Repulsion-based learning is used to update the populations' parameters that have been committed to memory.
- Select the mixed population based on fitness.
- Determine the objective function and show it.

2.3.2 IAOA

Summary of AOA

The foundation for basic mathematical operations, such as addition, subtraction, multiplication, and division, is arithmetic, a fundamental idea in modern mathematics rooted in number theory. These operations are used to assess numerical values and identify the maximum element within a set of solutions based on particular criteria [34]. These mathematical operations serve as the basis for the AOA, which is a tool for solving mathematical problems. AOA adheres to the standard population-based algorithm optimization

procedure, which includes the phases of exploration and exploitation. While exploitation concentrates on improving the accuracy of the solution, exploration attempts to thoroughly explore the search space [35]. The 3 main phases of AOA are explained in detail in the following sections.

Initialization

The first step in the optimization process of AOA involves creating a set of potential solutions (referred to as X) by chance. Each successive iteration is to result in that one candidate solution which is expected to be either the optimum solution, or at least the closest to it within a neighbourhood.

$$X = \begin{bmatrix} x_{1,1} & \cdots & x_{1,j} & \cdots & x_{1,n} \\ \cdots & \cdots & \cdots & \cdots & \cdots \\ x_{i,1} & \cdots & x_{i,j} & \cdots & x_{i,n} \\ \cdots & \cdots & \cdots & \cdots & \cdots \\ x_{N,1} & \cdots & x_{N,j} & \cdots & x_{N,n} \end{bmatrix} \quad (18)$$

It is necessary to choose in advance of beginning the AOA process, whether to start with either the exploration or exploitation phases. The function value at the i^{th} iteration is then calculated using the Math Optimizer Accelerated (MOA) function, which is defined by Eq. (19).

$$\text{MOA}(C_{it}) = \text{Min} + C_{it} \times \left(\frac{\text{Max} - \text{Min}}{M_{it}} \right) \quad (19)$$

The symbol M_{it} denotes the maximum number of repetitions. According to the accelerated function, Max and Min represent their highest and lowest values, respectively.

Exploration

In the research step, using Division (DO) or Multiplication (MO) operators, mathematical operations executed provide conclusions or judgments that are widely disseminated. While these actions perhaps do not approach the objective efficiently and can only converge toward a near-optimum solution after several rounds, they may simplify the shift to the exploitation phase. Equation (20) provides formulas for updating positions and outlines the 2 main search tactics used during exploration.

$$x'_{i,j} = \begin{cases} x_{b,j} \div (MOP + \varepsilon) \times ((ub_j - lb_j) \times \mu + lb_j), \\ r_2 < 0.5 \\ x_{b,j} \times MOP \times ((ub_j - lb_j) \times \mu + lb_j), \\ \text{otherwise} \end{cases} \quad (20)$$

It gives a straightforward method of creating neighboring solutions. Here, $x_{b,j}$ is the position at the j^{th} location of the presently best-acquired solution, $x'_{i,j}$ is the position at the j^{th} location of the i^{th} solution, ε is a small integer, and μ is a control parameter.

$MOP(C_{it})$ is indicated as follows:

$$MOP(C_{it}) = 1 - \left(\frac{C_{it}}{M_{it}} \right)^{1/\alpha} \quad (21)$$

In subsequent iterations of the exploitation process, the precision attained is controlled by a key parameter, represented by α .

Exploitation

The mathematical computations make use of operators like Subtraction (SO), and Addition (AO), to generate results of targeted outcomes during the exploitation phase. Through several iterations, these operators allow for efficient targeting of the desired outcome. The main search tactics and position update equations for this stage are given in Eq. (22). Meanwhile, the exploitation operators (SO and AO), help the implementation in finding the best solutions within related search techniques so that the system would not get trapped into local search areas.

$$x'_{i,j} = \begin{cases} x_{b,j} - MOP \times ((ub_j - lb_j) \times \mu + lb_j), & r_3 > 0.5 \\ x_{b,j} + MOP \times ((ub_j - lb_j) \times \mu + lb_j), & \text{otherwise} \end{cases} \quad (22)$$

A random quantity that is evenly split across [0,1] is denoted by r_3 .

Improved AOA (IAOA)

This conservative constraint can cause large movements in the solutions outside of the search space, where tight bounds are based on minor movements, risking early convergence into mediocre solutions. Moreover, when all the design variables take the same upper and lower bounds, as it is the case in discrete structural optimization using standard sections, AOA is confronted with some serious problems, which will be discussed in more detail.

An extensively known issue of the original AOA prematurely converges to poor solutions [36, 37]. Despite this, the AOA is still useful for examining search spaces. Because of the need for more investigation in the early phases of the search, variety is rapidly reduced, which is why this problem occurs [38]. Kaveh and Biabani Hamedani [38] created an enhanced version known as

IAOA in response to these drawbacks. The IAOA clearly distinguishes between the exploration and exploitation stages, each subject to different regulations regarding position updates, in contrast to the original AOA. As can be derived by Eq. (20), in AOA, during the exploration phase, most efforts will focus on the best-known solution that results in fast reduction of population diversity at the early stages of the search process. Furthermore, the efficiency of AOA during the exploration phase is strongly related to design variable constraints, which can cause problems with convergence when these bounds are very tight or wide. Large solution steps that may extend beyond the search space result from too conservative boundaries. However, modest steps produced by near constraints raise the possibility of an early convergence to unsatisfactory solutions. If all the design variables have the same bounds, as in discrete structural optimization involving standard sections, then an important problem that the original AOA faces will be discussed shortly.

The same adjustments are made to every feature of the best solution that has been found in each iteration, if $r_2 > 0.5$, as shown by Eq. (21) $(MOP + \varepsilon) \times ((ub_j - lb_j) \times \mu + lb_j)$. Similarly, in the best solution found so far, each design variable is scaled by the same factor $MOP \times ((ub_j - lb_j) \times \mu + lb_j)$. The research of AOAs is confined to a narrow region, as only two parameters drive all the design variables in the optimal solution during the first generation. It is quite common that because of the limited diversity, poor solutions converge slowly and prematurely [38]. This limitation also affects the original AOA throughout its exploitation phase (see Eq. (23)). IAOA has introduced a new position updating technique that makes use of division and multiplication operations [38] to address these problems in the exploration phase of the original AOA.

$$x'_{i,j} = \begin{cases} x_{i,j} \div (1 + (-1)^{\text{rand}_i([1,2])}) & 0.5 \times \text{rand} \times \overline{MOP}, \\ r_2 > 0.5 \\ x_{i,j} \times (1 + (-1)^{\text{rand}_i([1,2])}) & 0.5 \times \text{rand} \times \overline{MOP}, \\ \text{otherwise} \end{cases} \quad (23)$$

A pseudorandom number in [0–1] with a uniform distribution is represented by rand. For the i^{th} candidate solution, the present value of the j^{th} design variable is denoted by $x'_{i,j}$. A pseudorandom scalar number, 1 or 2, is produced by the function $\text{rand}_i([1,2])$. The parameter-free version of the function MOP , denoted by \overline{MOP} , is defined as follows [38]: The MOP function has a variation called \overline{MOP} that operates without the need for any further parameters.

$$\overline{MOP}(C_{it}) = \left(1 - \frac{C_{it}}{M_{it}}\right)^{\text{rand}_i([1,2])} \quad (24)$$

In contrast to original AOA, in the IAOA exploration phase, as represented by Eq. (20), it emphasizes the present position of the solutions. Essentially, the position of each solution is updated with respect to its current status in the IAOA exploration phase. This allows full exploration of the search space and avoids loss of diversity during the processes of the search [38]. Besides, using random numbers in Eqs. (23) and (24) results in the generation of various step sizes for moving solutions in the search space. The diversity of the population can be preserved and exploration is encouraged by this variation in step sizes [38]. The convergence-related problems may reduce as Eq. (22) is independent of the limits of design variables [38]. As demonstrated by Eq. (22), the original AOA's exploration and exploitation phases are centered on the best solution to date. When every design variable has the same upper and lower bounds during the exploitation phase, the primary issue occurs. The best solution lacks diversity because the same adjustment factor is applied to all design variables in each iteration, as shown by Eq. (22). This shows that the original AOA's exploitation phase, with equal limits of design variables, is not that efficient in investigating the search space. In order to overcome this limitation, IAOA uses subtraction and addition operators to develop a new position updating algorithm for the exploitation phase [38].

$$x'_{i,j} = \begin{cases} b(x_j) - b(x_j) \times \text{rand} \times \overline{MOP} \times (UB_j - LB_j), \\ r_3 > 0.5 \\ b(x_j) + b(x_j) \times \text{rand} \times \overline{MOP} \times (UB_j - LB_j), \\ \text{otherwise} \end{cases} \quad (25)$$

By generating variable step sizes for solution movement, Eqs. (24) and (25) enhance the use of the optimal solution. On the other hand, each application requires the original AOA to be tuned for 4 different parameters (Min, Max, α , and μ), and $b(x_j)$ denoted the best x_j . The implementation of IAOA is remarkably made simpler by eliminating the terms α and μ from its formulation.

2.4 Evaluation metrics

Regression models are evaluated using a number of measures that quantify their performance and accuracy. The R^2 has values between 0 and 1, where 1 denotes a perfect fit, and it quantifies how well the independent factors account for the variability of the dependent variable. There are two measures to quantify the prediction error,

namely RMSE and MAE. Because the RMSE represents the square root of the average squared differences between the observed value and projected value, this is sensitive to outliers, while the MAE returns a more robust measure of the metric. The n10-index, sometimes referred to as top-decile lift, in general use in marketing and finance to identify best performers, relates to a measure of a model's performance to predict the top 10 percent of the values. Finally, MARE (Mean Absolute Relative Error) normalizes errors by taking the mean of the absolute values of the relative errors, which makes it possible to make comparisons across different scales or different models. Each one of these indicators brings different information on model performance and thus can be useful for a range of evaluation purposes according to the specific goals and characteristics that a regression problem might have:

$$R^2 = \left(\frac{\sum_{i=1}^n (a_i - \bar{a})(b_i - \bar{b})}{\sqrt{\left[\sum_{i=1}^n (a_i - \bar{a})^2 \right] \left[\sum_{i=1}^n (b_i - \bar{b})^2 \right]}} \right)^2 \quad (26)$$

$$\text{RMSE} = \sqrt{\frac{1}{n} \sum_{i=1}^n (b_i - a_i)^2} \quad (27)$$

$$\text{MAE} = \frac{1}{n} \sum_{i=1}^n |b_i - a_i| \quad (28)$$

$$\text{n10-index} = \frac{n10}{n} \quad (29)$$

$$\text{MARE} = \frac{1}{n} \sum_{i=1}^n \frac{|b_i - a_i|}{a_i} \quad (30)$$

where n is the number of data points, a is the measured data, b represents the predicted data, \bar{a} is the average of the measured data and \bar{b} is the forecasted data, respectively.

3 Results and discussion

Fig. 2 presents the convergence curve graph of RMSE from two hybrid models: SGSB and SGIA. The graph plots the RMSE with respect to iterations: green corresponds to the SGIA method, while pink corresponds to the SGSB algorithm. Both algorithms show a decreasing RMSE with more iterations, showing an improvement in their predicting accuracy. Additionally, after about 125 cycles, both algorithms converge to their lowest RMSE values. The SGSB algorithm converges to a little higher RMSE of 0.150, whereas the SGIA algorithm's ultimate RMSE is 0.114. The SGIA algorithm works better than the SGSB algorithm, achieving a lower error rate, since a lower RMSE denotes better model performance. Based on its lower final RMSE, SGIA emerges as the better model, effectively highlighting the convergence behavior and relative accuracy of the two algorithms in this graph.

Of the three models examined in Table 2, the SGIA model performs the best according to a number of

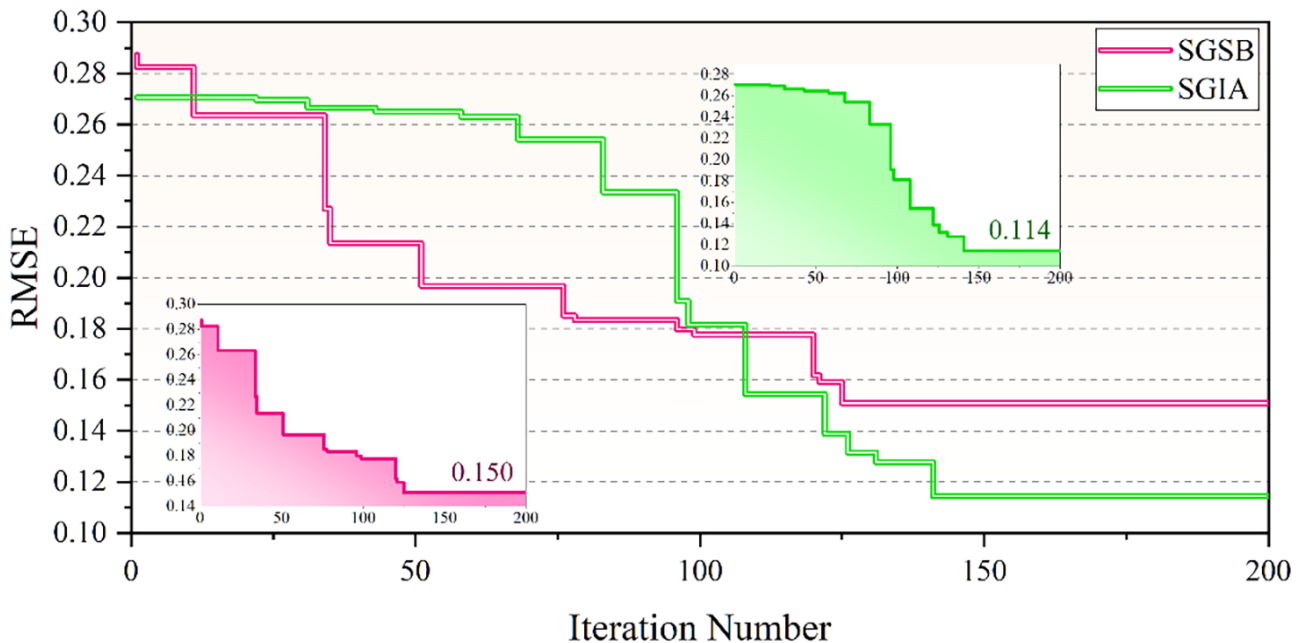


Fig. 2 The convergence curve of the 4 hybrid models presented

Table 2 The result of developed models for SGB

| Phase | Model | Index values | | | | | Ranking the predicted model | | | | | Total ranking score |
|------------|-------|--------------|-------|-------|-----------|-------|-----------------------------|-------|-----|-----------|------|---------------------|
| | | RMSE | R^2 | MAE | n10-index | MARE | RMSE | R^2 | MAE | n10-index | MARE | |
| Train | SGSB | 0.136 | 0.983 | 0.119 | 0.980 | 0.034 | 2 | 2 | 2 | 2 | 2 | 10 |
| | SGIA | 0.093 | 0.991 | 0.080 | 1.000 | 0.023 | 3 | 3 | 3 | 3 | 3 | 15 |
| | SGB | 0.188 | 0.964 | 0.156 | 0.952 | 0.043 | 1 | 1 | 1 | 1 | 1 | 5 |
| Validation | SGSB | 0.198 | 0.970 | 0.144 | 0.969 | 0.035 | 2 | 2 | 2 | 2 | 2 | 10 |
| | SGIA | 0.161 | 0.981 | 0.119 | 1.000 | 0.031 | 3 | 3 | 3 | 3 | 3 | 15 |
| | SGB | 0.265 | 0.960 | 0.209 | 0.875 | 0.052 | 1 | 1 | 1 | 1 | 1 | 5 |
| Test | SGSB | 0.161 | 0.974 | 0.128 | 0.968 | 0.036 | 2 | 2 | 2 | 2 | 2 | 10 |
| | SGIA | 0.144 | 0.980 | 0.113 | 0.968 | 0.033 | 3 | 3 | 3 | 3 | 3 | 15 |
| | SGB | 0.227 | 0.949 | 0.197 | 0.903 | 0.059 | 1 | 1 | 1 | 1 | 1 | 5 |
| All | SGSB | 0.151 | 0.977 | 0.124 | 0.976 | 0.035 | 2 | 2 | 2 | 2 | 2 | 10 |
| | SGIA | 0.114 | 0.986 | 0.091 | 0.995 | 0.026 | 3 | 3 | 3 | 3 | 3 | 15 |
| | SGB | 0.208 | 0.959 | 0.170 | 0.933 | 0.047 | 1 | 1 | 1 | 1 | 1 | 5 |

assessment indicators (SGSB, SGIA, and SGB). By analyzing the training phase SGIA has the highest R^2 value (0.991), which indicates that it has an exceptional predictive ability (99.1% of the variability in the dependent variable is explained by it). SGIA likewise has the highest n10-index (1.000), demonstrating its exceptional capacity to identify the top 10% of values. With the lowest error metrics values throughout the article, SGIA performs exceptionally well. It attains an RMSE of 0.093, indicating low average prediction error and a high degree of accuracy. Similarly, by averaging the absolute differences between predicted and actual values, SGIA's MAE of 0.080 highlights its robust performance. To highlight the accuracy of the model, the MARE for SGIA is 0.023, which normalizes the errors in relation to the real values. SGIA has a total ranking score of 15, which places it third overall. Because of its exceptional performance in important metrics like R^2 , RMSE, MAE, and MARE, it is regarded as the best model in this article. Out of the 3 models that were evaluated, SGIA was found to be the most reliable and accurate due to its combined high R^2 and n10-index, as well as its lowest error values.

In Fig. 3, a diagonal line appears in all three models, symbolizing the optimal situation in which $R^2 = 1$ and $RMSE = 0$ signify flawless alignment of prediction and measurement. Furthermore, two lines are shown with a 10% error margin at +10% and -10% from this baseline. The better model is the one with more data points that are nearer this baseline. SGIA is the most excellent model among those evaluated; it is evident from the large concentration of data points it has close to the baseline. During the training phase, SGIA specifically achieves an R^2 value of 0.991 and an RMSE of 0.093. SGIA is the best model in the

study because its data points are close to the ideal diagonal line, which highlights its low error rate and high reliability.

The data points are graphically represented in Fig. 4 so that the degree of agreement between the measured and predicted values for each parameter can be evaluated. A greater degree of consistency between the measured values and the predicted data points is a sign of a better-performing model. Fig. 4 makes it clear that the single SGB model is the weakest of the models examined because it shows notable differences between predicted and measured values. The greatest degree of agreement between predicted and measured data points, however, is shown by the SGIA model. The SGIA model is the most successful model in the study, as further proof of its superior performance comes from its alignment with the measured data. This consistency, both quantitatively and visually, establishes SGIA as the best model, surpassing other models in terms of overall efficacy and predictive accuracy.

Sample numbers are represented on the X-axis and error percentages are represented on the Y-axis in the error plots for the 3 models (SGSB, SGIA, and SGB) that show the error percentage over various data samples in Fig. 5. Each plot uses different colors to indicate which data are test, validation, and training. The maximum error of 11.76% is found in Fig. 5 (a), which shows the SGSB model's error percentage, and it happens close to sample number 150. This suggests that even though the SGSB model functions well most of the time, there is a noticeable peak in error around this sample, which represents a brief loss in accuracy. Fig. 5 (b) displays the SGIA model's error percentage. The highest error that has been noted in this case is 13.29%, and it occurs at sample number 190. The robust

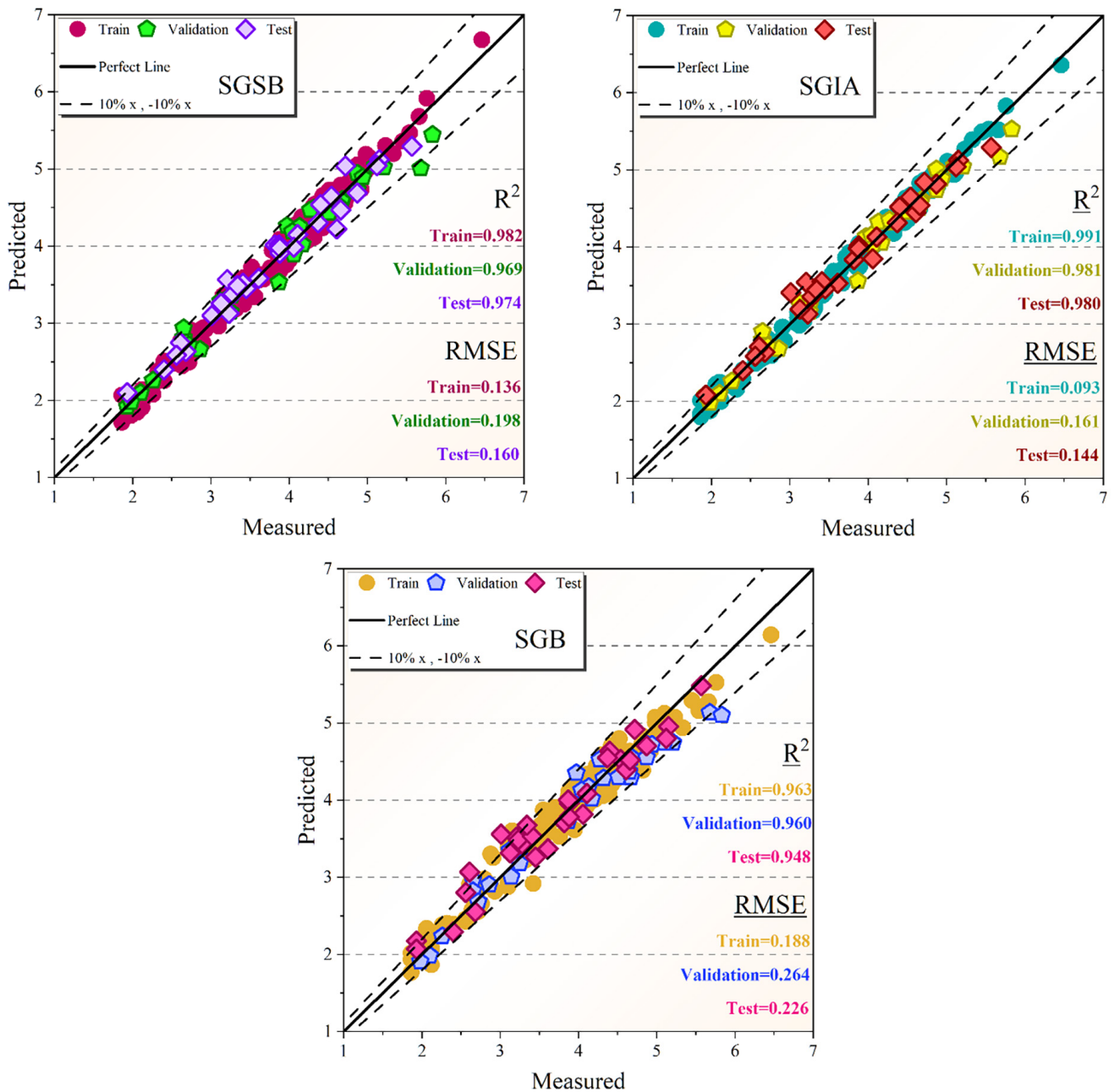


Fig. 3 The dispersion of evolved hybrid models

performance and consistency in prediction accuracy of the SGIA model are demonstrated by its ability to maintain a relatively low and stable error percentage across different samples, even in the face of this peak. The SGB model, which has the largest maximum error of the 3 models at 18.22%, likewise around sample number 190, is represented by the error percentage for the model in Fig. 5 (c). This notable error peak highlights the relative weakness of the SGB model by showing that it struggles with accuracy more than the SGSB and SGIA, especially around this sample. The SGIA model outperforms the others in terms of predictive accuracy, as demonstrated by these

plots, which show that although each model has occasional periods of greater error, overall performance is generally more stable and error rates are lower. In comparison to the SGB model, which shows the highest error and thus a relatively poorer performance, the SGSB model performs reasonably well but has a less clear error peak.

The distribution of errors for three ML models is shown in Fig. 6. To show these errors as percentages, violin plots are created by blending box plots with density plots. The width of each violin plot creates a dramatic picture of the distribution of error in each model's performance by essentially reflecting the density of data points showing up

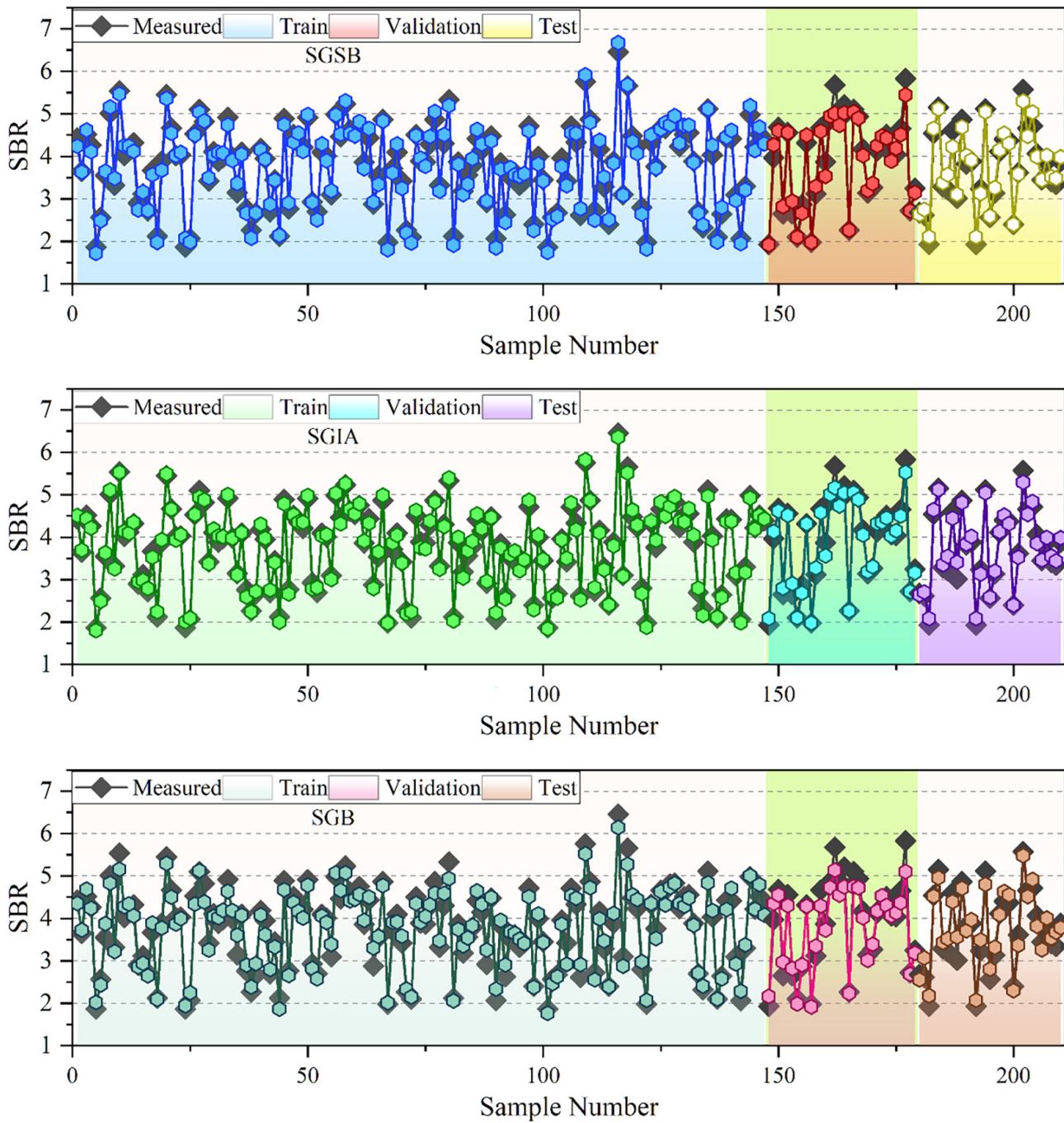
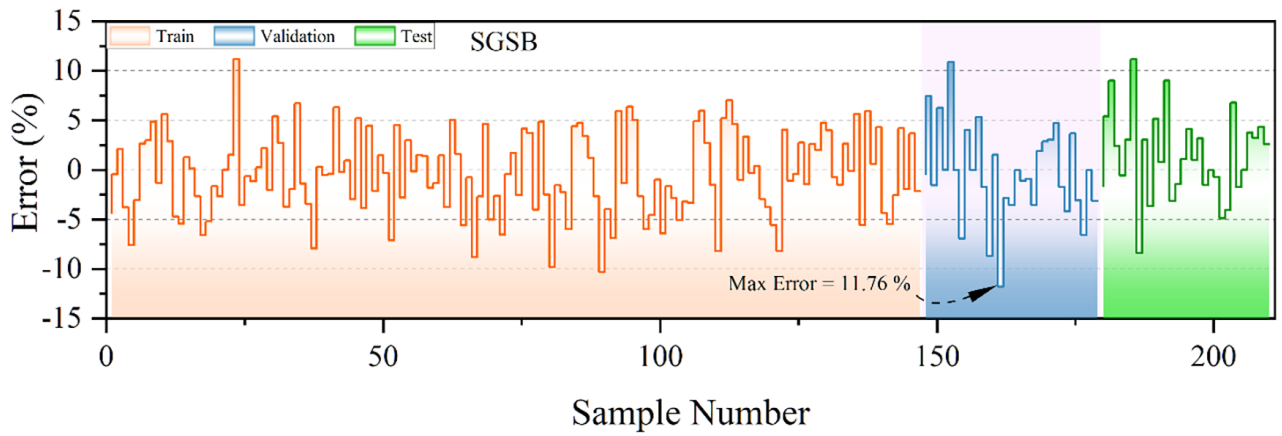


Fig. 4 The metric of predicted and measured values

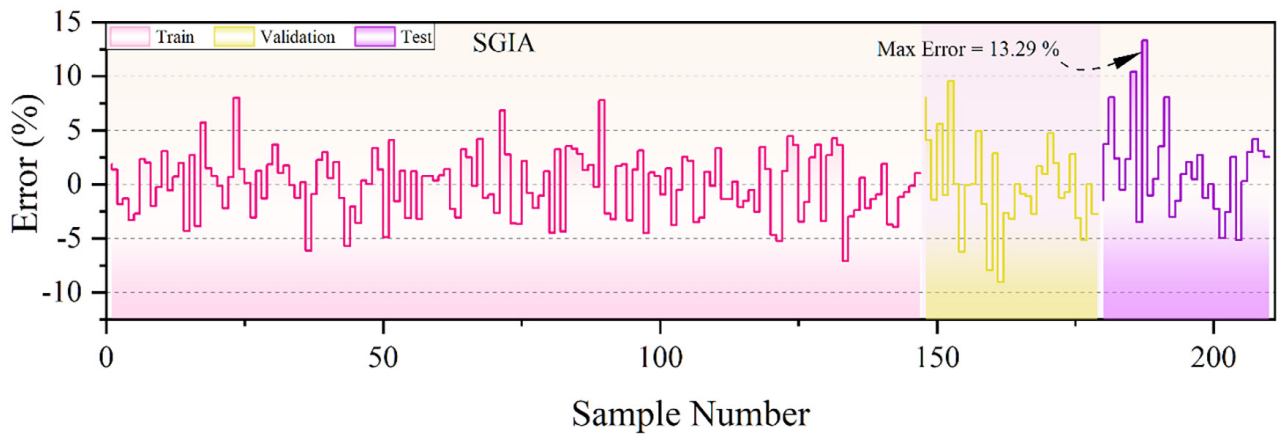
around a specific percentage of error. First of all, the SGIA model's violin plot illustrates high density within the zero error percentage, with most of the model's predictions being extremely accurate. The violin plot of the SGIA shows that the concentrations of low error levels are high, reflecting that this algorithm performs well and is reliable on all datasets when it comes to reducing prediction error. Whereas SGSB and SGB models showed a wider range in the violin plots with a fewer numbers of data points clustered around zero, indicating that because these models

have larger variable error rates, their prediction accuracy is not that reliable. Fig. 6 has the highest density of data points at low error percentages and therefore represents the best error distribution for SGIA overall.

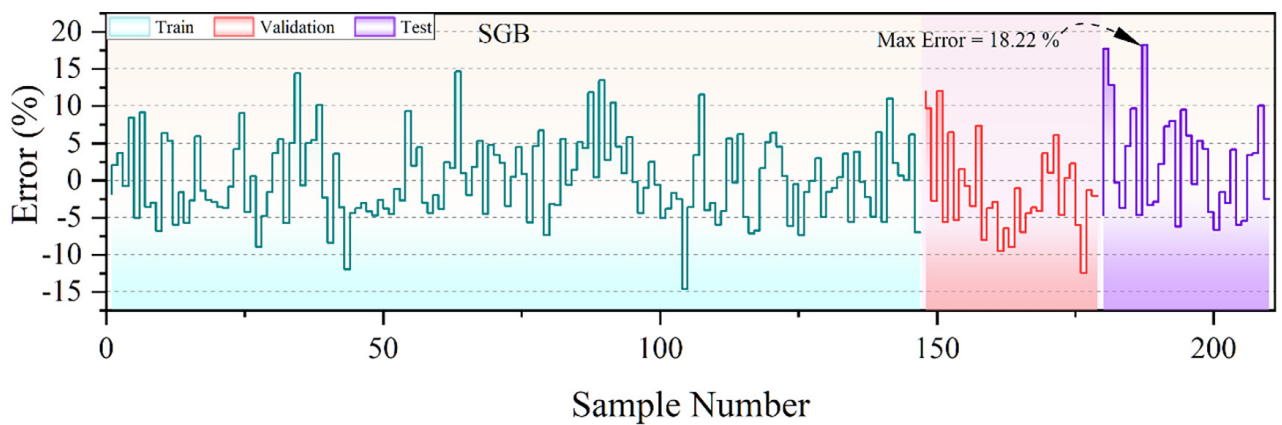
Fast Sensitivity Analysis (FSA) is a simplified technique of how the outputs of a model would be affected by changes in input parameters. Because it is highly effective and scalable, FSA can be nicely applied to complicated models that contain large numbers of parameters. FSA employs mathematical processes to measure the sensitivities of each



(a)



(b)



(c)

Fig. 5 The error percentage of the models (a) SGSB, (b) SGIA, and (c) SGB is based on the vertical plot

input parameter using standardized regression coefficients or partial derivatives. Its ease of execution and interpretation means key factors possibly having the most substantial impact on model outcomes can quickly be identified. Applications that FSA finds in engineering, economics, and environmental sciences are employed to make better decisions, validate models, and optimize them.

While the total effect index, ST, considers interaction effects in addition to the direct influence of that input variable, the first-order sensitivity index, S1 in quick sensitivity analysis characterizes the variance in output that can be directly related to a single input variable. The present study identifies the most vital elements needed for the prediction of the CBR values. As can be seen from Fig. 7, the

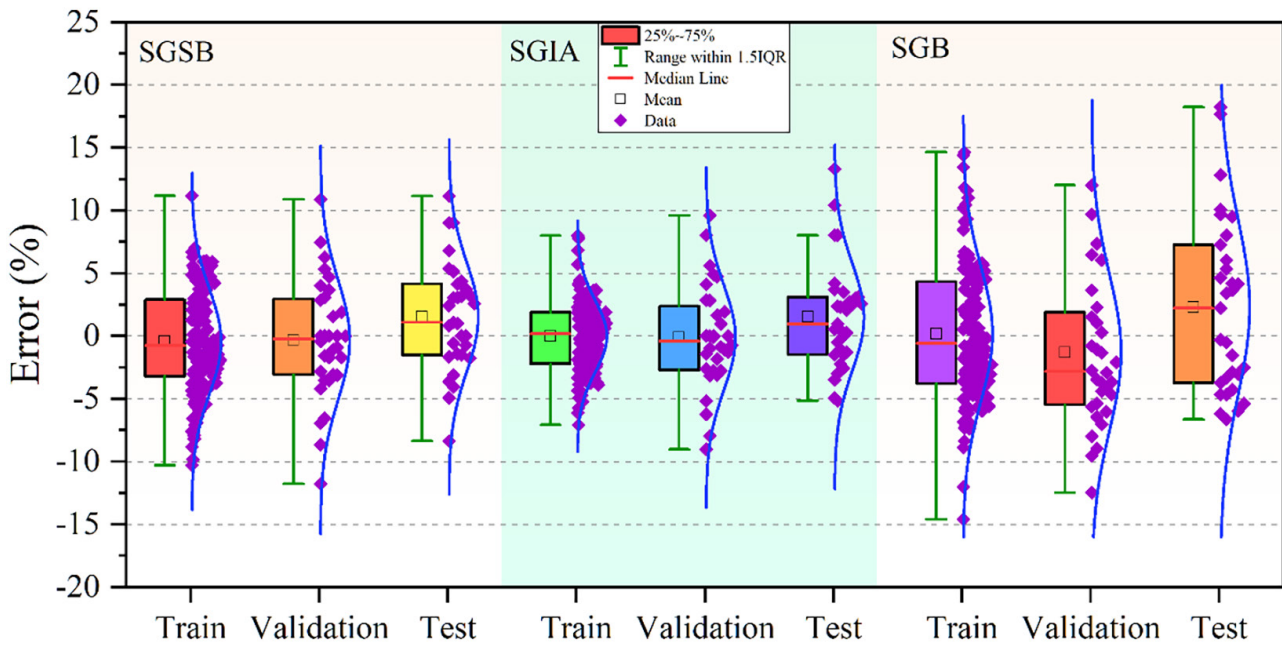


Fig. 6 The box with symbol plot errors of proposed models

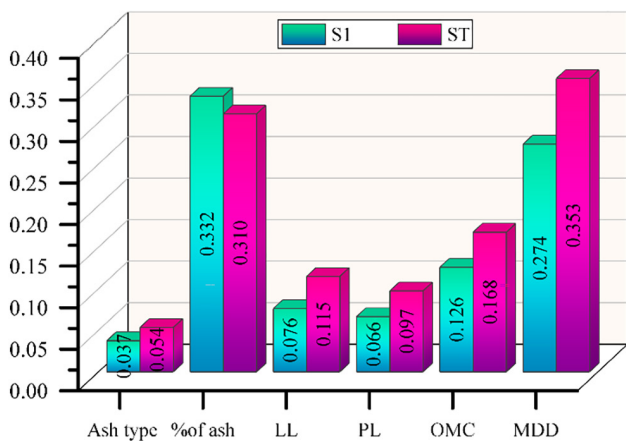


Fig. 7 The fast sensitivity analysis of the best-performed model

Maximum Dry Density (MDD) parameter has the highest ST value of 0.353, indicating that it has the greatest overall impact on the output, including interactions. The high S1 value of 0.332 corresponds to the ash percentage, which has a large effect on the CBR estimate. The second highest values of both ST and S1, with 0.310 and 0.274 respectively, correspond to ash percentage and the MDD parameter. To develop effective strategies for modeling and optimization, an understanding is required about which variables provide the most impacts on the CBR values.

4 Conclusions

This paper proved that advanced machine learning algorithms work in the estimation of CBR values, which are significant in civil engineering, especially in road and

pavement construction. Two hybrid models, SGIA and SGSB, were advanced through IAOA and SBOA optimization procedures, respectively, for building and assessment using the SGBR model. These included the n10-index, Mean Absolute Error (MAE), RMSE, R^2 , and MARE. Testing consisted of (15%), validation was (15%), while training consisted of (70%) of the dataset. This form of segmentation has been crucial in ensuring that the models are well trained to capture all the important features of the data and that they are well tested for their accuracy and strength. Numerically and visually, too, the SGIA model outperformed the SGSB model. That means the performance of the SGIA model outperformed the SGSB model by 0.92%, with its R^2 score at 0.986. The model also produced an n10-index of 0.995 for the SGIA model, which was 1.95% higher than the SGSB model. The model further presented the minimum error metrics with RMSE of 0.114 and MAE and MARE of 0.091 and 0.026, respectively, showing that the model carried out its predictions of CBR values with excellent accuracy and reliability. It is expected that the outcome of this work will provide a reliable and rapid method of calculating the CBR values of soil, which considerably affects civil engineering. Thus, accurate CBR estimates are of high importance to better planning and construction of pavement and road structures, hence stability and lifetime under optimized use of resources. The hybrid models developed in this research, especially the SGIA, can be utilized by engineers in making better decisions, cutting costs, and further increasing the sustainability of building projects.

References

- [1] Selcer, P. "The Postwar Origins of the Global Environment: How the United Nations Built Spaceship Earth", [e-book] Columbia University Press, 2018. ISBN 9780231548236
<https://doi.org/10.7312/selc16648>
- [2] Bulkeley, H., Betsill, M. "Rethinking sustainable cities: Multilevel governance and the 'urban' politics of climate change", *Environmental Politics*, 14(1), pp. 42–63, 2005.
<https://doi.org/10.1080/0964401042000310178>
- [3] Beatley, T. "Green urbanism: Learning from European cities", [e-book] Island Press, 2012. ISBN 9781610910132
- [4] Kennedy, C., Cuddihy, J., Engel-Yan, J. "The changing metabolism of cities", *Journal of Industrial Ecology*, 11(2), pp. 43–59, 2007.
<https://doi.org/10.1162/jie.2007.1107>
- [5] Amakye, S. Y., Abbey, S. J. "Understanding the performance of expansive subgrade materials treated with non-traditional stabilisers: A review", *Cleaner Engineering and Technology*, 4, 100159, 2021.
<https://doi.org/10.1016/j.clet.2021.100159>
- [6] Faeq, R. H. F. "Compaction and CBR properties of reclaimed asphalt pavement mixed with sand", MSc Thesis, Hasan Kalyoncu University, 2016.
- [7] Zhou, Z., Bai, R., Shen, M., Wang, Q. "The effect of overconsolidation on monotonic and cyclic behaviours of frozen subgrade soil", *Transportation Geotechnics*, 32, 100710, 2022.
<https://doi.org/10.1016/j.trgeo.2021.100710>
- [8] Fuentes, W., Duque, J., Lascarro, C., Gil, M. "Study of the bearing capacity of closely spaced square foundations on granular soils", *Geotechnical and Geological Engineering*, 37(3), pp. 1401–1410, 2019.
<https://doi.org/10.1007/s10706-018-0694-5>
- [9] Polo-Mendoza, R., Duque, J., Mašín, D., Turbay, E., Acosta, C. "Implementation of deep neural networks and statistical methods to predict the resilient modulus of soils", *International Journal of Pavement Engineering*, 24(1), 2257852, 2023.
<https://doi.org/10.1080/10298436.2023.2257852>
- [10] Mašín, D. "Modelling of soil behaviour with hypoplasticity: Another approach to soil constitutive modelling", *Springer Series in Geomechanics and Geoengineering*, Springer, 2019. ISBN 978-3-030-03975-2
<https://doi.org/10.1007/978-3-030-03976-9>
- [11] Izquierdo, M., Querol, X., Vazquez, E. "Procedural uncertainties of Proctor compaction tests applied on MSWI bottom ash", *Journal of Hazardous Materials*, 186(2–3), pp. 1639–1644, 2011.
<https://doi.org/10.1016/j.jhazmat.2010.12.045>
- [12] Cerni, G., Camilli, S. "Comparative analysis of gyratory and proctor compaction processes of unbound granular materials", *Road Materials and Pavement Design*, 12(2), pp. 397–421, 2011.
<https://doi.org/10.1080/14680629.2011.9695251>
- [13] Čápayová, S., Štefunková, Z., Unčík, S., Zuzulová, A. "Requirements for pavement base layers with unbound granular material", *Slovak Journal of Civil Engineering*, 27(3), pp. 21–28, 2019.
<https://doi.org/10.2478/sjce-2019-0018>
- [14] Mukherjee, S., Ghosh, P. "Soil Behavior and Characterization: Effect of Improvement in CBR Characteristics of Soil Subgrade on Design of Bituminous Pavements", *Indian Geotechnical Journal*, 51(3), pp. 567–582, 2021.
<https://doi.org/10.1007/s40098-021-00533-8>
- [15] Raju, Y. K., Kumar, C. V. "Experimental Investigation on Design of Thickness for Flexible Pavement Subgrade Soils using CBR Approach", *E3S Web of Conferences*, 184, 01087, 2020.
<https://doi.org/10.1051/e3sconf/202018401087>
- [16] Haghighi, H., Arulrajah, A., Mohammadinia, A., Horpibulsuk, S. "A new approach for determining resilient moduli of marginal pavement base materials using the staged repeated load CBR test method", *Road Materials and Pavement Design*, 19(18), pp. 1848–1867, 2018.
<https://doi.org/10.1080/14680629.2017.1352532>
- [17] Acheampong, A. O., Dzor, J., Dzor, M., Salim, R. "Unveiling the effect of transport infrastructure and technological innovation on economic growth, energy consumption and CO₂ emissions", *Technological Forecasting and Social Change*, 182, 121843, 2022.
<https://doi.org/10.1016/j.techfore.2022.121843>
- [18] Kaveh, A. "Applications of artificial neural networks and machine learning in civil engineering", Springer, 2024. ISBN 978-3-031-66050-4
<https://doi.org/10.1007/978-3-031-66051-1>
- [19] Munday, M., Reynolds, L., Roberts, A. "Re-appraising 'in-process' benefits of strategic infrastructure improvements: Capturing the unexpected socio-economic impacts for lagging regions", *Transport Policy*, 134, pp. 119–127, 2023.
<https://doi.org/10.1016/j.tranpol.2023.02.012>
- [20] Duque, J., Fuentes, W., Rey, S., Molina, E. "Effect of grain size distribution on California bearing ratio (CBR) and modified proctor parameters for granular materials", *Arabian Journal for Science and Engineering*, 45(10), pp. 8231–8239, 2020.
<https://doi.org/10.1007/s13369-020-04673-6>
- [21] Farooq, K., Mujtaba, H. "Prediction of California Bearing Ratio (CBR) and Compaction Characteristics of Granular Soils", *Acta Geotechnica Slovenica*, 14(1), pp. 63–72, 2017.
- [22] Jong, S. C., Ong, D. E. L., Oh, E. "State-of-the-art review of geotechnical-driven artificial intelligence techniques in underground soil-structure interaction", *Tunnelling and Underground Space Technology*, 113, 103946, 2021.
<https://doi.org/10.1016/j.tust.2021.103946>
- [23] Sharma, S., Ahmed, S., Naseem, M., Alnumay, W. S., Singh, S., Cho, G. H. "A survey on applications of artificial intelligence for pre-parametric project cost and soil shear-strength estimation in construction and geotechnical engineering", *Sensors*, 21(2), 463, 2021.
<https://doi.org/10.3390/s21020463>
- [24] Baghbani, A., Choudhury, T., Costa, S., Reiner, J. "Application of artificial intelligence in geotechnical engineering: A state-of-the-art review", *Earth-Science Reviews*, 228, 103991, 2022.
<https://doi.org/10.1016/j.earscirev.2022.103991>
- [25] Yin, Z., Jin, Y., Liu, Z. "Practice of artificial intelligence in geotechnical engineering", *Journal of Zhejiang University-Science A*, 21(6), pp. 407–411, 2020.
<https://doi.org/10.1631/jzus.A20AIGE1>
- [26] Jaksa, M., Liu, Z. "Editorial for special issue "Applications of artificial intelligence and machine learning in geotechnical engineering"", *Geosciences*, 11(10), 399, 2021.
<https://doi.org/10.3390/geosciences11100399>
- [27] Breiman, L. "Bagging predictors", *Machine Learning*, 24(2), pp. 123–140, 1996.
<https://doi.org/10.1007/BF00058655>

- [28] Freund, Y., Schapire, R. E. "Experiments with a new boosting algorithm", In: Proceedings of the Thirteenth International Conference on International Conference on Machine Learning, Bari, Italy, 1996, pp. 148–156. ISBN 1558604197
- [29] Breiman, L. "Using adaptive bagging to debias regressions", Statistics Department, University of California at Berkeley, Berkeley, CA, USA, Technical Report 547, 1999.
- [30] Friedman, J. H. "Greedy function approximation: A gradient boosting machine", *The Annals of Statistics*, 29(5), pp. 1189–1232, 2001. <https://doi.org/10.1214/aos/1013203451>
- [31] Das, A. K., Pratihar, D. K. "A new bonobo optimizer (BO) for real-parameter optimization", In: 2019 IEEE Region 10 Symposium (TENSYPMP), Kolkata, India, 2019, pp. 108–113. ISBN 978-1-7281-0298-6 <https://doi.org/10.1109/TENSYPMP46218.2019.8971108>
- [32] Farh, H. M. H., Al-Shamma'a, A. A., Al-Shaalan, A. M., Alkuhayli, A., Noman, A. M., Kandil, T. "Technical and economic evaluation for off-grid hybrid renewable energy system using novel bonobo optimizer", *Sustainability*, 14(3), 1533, 2022. <https://doi.org/10.3390/su14031533>
- [33] Abdelghany, R. Y., Kamel, S., Sultan, H. M., Khorasy, A., Elsayed, S. K., Ahmed, M. "Development of an improved bonobo optimizer and its application for solar cell parameter estimation", *Sustainability*, 13(7), 3863, 2021. <https://doi.org/10.3390/su13073863>
- [34] Habib, M. K., Cherri, A. K. "Parallel quaternary signed-digit arithmetic operations: addition, subtraction, multiplication and division", *Optics & Laser Technology*, 30(8), pp. 515–525, 1998. [https://doi.org/10.1016/S0030-3992\(99\)00004-3](https://doi.org/10.1016/S0030-3992(99)00004-3)
- [35] Abualigah, L., Diabat, A., Mirjalili, S., Abd Elaziz, M., Gandomi, A. H. "The arithmetic optimization algorithm", *Computer Methods in Applied Mechanics and Engineering*, 376, 113609, 2021. <https://doi.org/10.1016/j.cma.2020.113609>
- [36] Xu, Y.-P., Tan, J.-W., Zhu, D.-J., Ouyang, P., Taheri, B. "Model identification of the proton exchange membrane fuel cells by extreme learning machine and a developed version of arithmetic optimization algorithm", *Energy Reports*, 7, pp. 2332–2342, 2021. <https://doi.org/10.1016/j.egy.2021.04.042>
- [37] Abualigah, L., Diabat, A., Sumari, P., Gandomi, A. H. "A novel evolutionary arithmetic optimization algorithm for multilevel thresholding segmentation of COVID-19 CT images", *Processes*, 9(7), 1155, 2021. <https://doi.org/10.3390/pr9071155>
- [38] Kaveh, A., Biabani Hamedani, K. "Improved arithmetic optimization algorithm and its application to discrete structural optimization", *Structures*, 35, pp. 748–764, 2022. <https://doi.org/10.1016/j.istruc.2021.11.012>